Chinese Chemical Letters 34 (2023) 107517

Contents lists available at ScienceDirect

Chinese Chemical Letters

journal homepage: www.elsevier.com/locate/cclet

The development of an iridium(III) complex functionalized G-quadruplex probe for the stability of G-quadruplex and lifetime image in cytoplasm

Shaokang Jia[a,1], Wenjin Wang[b,1], Shanshan Qin[a], Shengjie Xie[a], Lisi Zhan[a], Qi Wei[a], Ziang Lu[a], Xiaolu Zhou[a], Cong Chen[a], Kun Chen[a], Shen Yan[a], Caiping Tan[b], Zongwan Mao[b,*], Xiang Zhou[a,*]

[a] College of Chemistry and Molecular Sciences, Key Laboratory of Biomedical Polymers-Ministry of Education, Wuhan University, Wuhan 430072, China
[b] MOE Key Laboratory of Bioinorganic and Synthetic Chemistry, School of Chemistry, Sun Yat-sen University, Guangzhou 510275, China

ARTICLE INFO

Article history:
Received 7 February 2022
Revised 7 May 2022
Accepted 10 May 2022
Available online 14 May 2022

Keywords:
G-quadruplex
Pyridostatin derivatives
Iridium(III) complex
Phosphorescent probe
Phosphorescence lifetime
Cell imaging

ABSTRACT

G-quadruplex (G4) is widely known as a non-classical secondary structure of nucleic acid. With the in-depth study of G4, it is an urgent need for a phosphorescent probe with a high G4 binding ability to evaluate the level of G4 in the cytoplasm. Thus, this study designed and synthesized **Ir-PDP** where an Ir(III) complex was used as a phosphorescent emitter. Meanwhile, two installed PDPs (pyridostatin derivatives) were used to improve the combination ability with G4 and reduced the cytotoxicity of the Ir(III) complex. Compared with other nucleic acid secondary structures, **Ir-PDP** produced a higher phosphorescence lifetime after interacting with G4. **Ir-PDP** was distributed in the cytoplasm of living cells, and two-photon phosphorescence lifetime imaging can detect the binding events of the probe in the cytoplasm. The addition of G4 binder PDS significantly regulated cytoplasmic phosphorescence lifetime. The project explored a new sensing pathway to observe the binding manners of probes in the cytoplasm through the phosphorescence lifetime of probes.

Guanine can simultaneously show the properties of both hydrogen bond donor and acceptor. As a result, in addition to the classical Watson–Crick hydrogen bonds, G-rich nucleic acid sequences can fold up into G-quartets with a planar structure that can form G-quadruplex (G4) through $\pi-\pi$ stacking interactions [1,2]. Compared with complementary base pairing, the enlarged planar structure formed by the Hoogsteen hydrogen bonds makes it easier for small molecules with an optimal electronic density of the aromatic surface to selectively bind to G-quadruplex through $\pi-\pi$ interactions [3,4]. Both DNA and RNA G4 provide crucial formation mechanisms and regulation functions in cell biological processes [5]. In addition, G4 structures in the cytoplasm participate numerous metabolic processes, such as repressing the translation of mRNA [6–8] and regulating Dicer-mediated cleavage [9]. Given the multitudinous effects of G4 on physiological activities, there is a need for developing a simple tool to detect G4 levels in the cytoplasm. The existence of folded RNA G4 in the cytoplasm has been confirmed by RNA G4 immunofluorescence imaging [10], fluorescent gene hybridization probe [11], and small molecule fluorescence localization imaging [12–17].

Moreover, the developments of luminescence lifetime bioimaging probes make it becomes possible to image without the interference of endogenous bioluminescence [18]. For instance, a low-concentration probe provides a key function in DNA G4 kinetic level detection by the adjustment of exposure time [19]. Furthermore, the fluorescence lifetime of the probe combined with DNA G4 can be directly tested for fluorescence lifetime imaging of G4 in living cells [20–23]. However, there are few reports on the phosphorescence lifetime imaging of G4 in the cytoplasm of living cells.

The lifetimes of the probes for the fluorescence lifetime imaging microscopy (FLIM) are usually similar to that of the cell background autofluorescence. And the emission lifetime of metal complexes can be extended to the microseconds range, which is attributed to the high spin-orbit coupling of heavy metal ions. Therefore, metal complexes with long lifetime emission are ideal candidates for photoluminescence lifetime imaging microscopy (PLIM) [24]. Moreover, the microenvironment-sensitive properties of

* Corresponding authors.
E-mail addresses: cesmzw@mail.sysu.edu.cn (Z. Mao), xzhou@whu.edu.cn (X. Zhou).
[1] These authors contributed equally to this work.

https://doi.org/10.1016/j.cclet.2022.05.031
1001-8417/

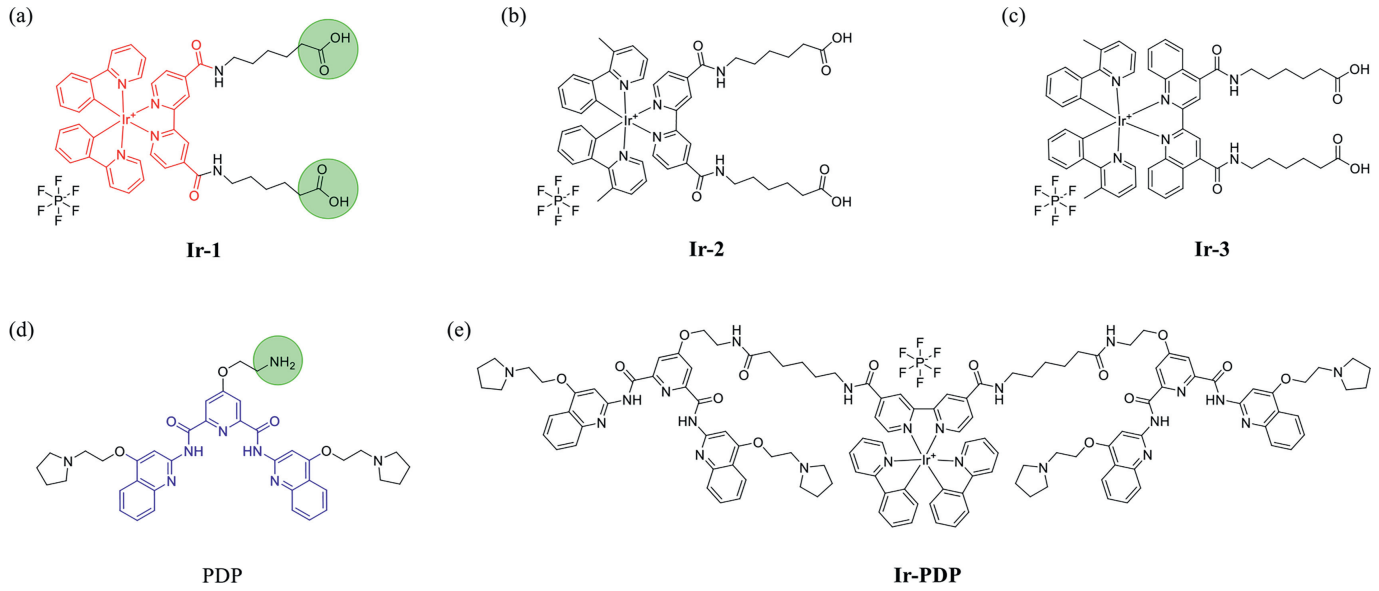

Fig. 1. Chemical structures of the Ir(III) complex scaffolds and G4 ligand PDP. (a-c) Chemical structures of the Ir(III) complex scaffolds under study in this work. Carboxyl groups that can be used for subsequent modification are highlighted in the green circle. (d) Chemical structures of PDP. The green circle emphasizes the amino group that can be used to connect the phosphorescent scaffold. (e) Chemical structures of **Ir-PDP**.

phosphorescence metal complexes make them be suitable probes for discriminating changes of the cellular physiological condition [25–27]. Although the metal complexes have excellent luminescence properties, their toxicity and limited nuclear membrane penetration often create adverse effects on bioimaging. As a result, many metal complexes with G4 response *in vitro* have not been used in live-cell G4 imaging [28–31].

PDP is an easily modified G4 ligand. Zhou and his co-workers have successfully used it to pull down proteins related to G4 structures both outside and inside cells, which is related to the good G4 affinity of PDP [32,33]. Therefore, attaching the ligand PDP that can interact with the G4 plane to the iridium(III) complex with long-lifetime phosphorescence will develop a probe, which is expected to image G4 structure in cells by phosphorescence lifetime. The phosphorescence lifetime signal may be independent of the phosphorescence intensity of the probe in the cell, which provides a new perspective for establishing the relationship between the structure and function of the G4 sequence in living cells.

In this study, an **Ir-PDP** complex, which works as a cytoplasm G4 imaging probe has been synthesized. The substituents with high steric hindrance reduce the non-specific binding of probes in the cytoplasm, which, as a result, reduced the toxicity caused by heavy metal complexes [34,35].

In this case, **Ir-1**–**Ir-3** (Figs. 1a-c) were obtained by the condensation between aminocaproic acid and the carboxylic groups attached to the N^N ligand of Ir(III) complexes. The long-chain linker is used as aminocaproic acid, which can reduce the interference of the Ir(III) complex on the binding of PDP (Fig. 1d) and G4, in addition, its length can still promote the interaction between Ir(III) complex and G4 [19]. The Ir(III) complexes were explored only by adding electron-donor groups such as methyl and phenyl based on 2-phenylpyridine and 2,2′-bipyridine. This is because *in vitro* findings indicate that adding electron-withdrawing groups reduce the complex response to G4 [28]. The UV–vis absorption spectra and phosphorescence emission intensity of different Ir(III) complexes were used as a test of their suitability. Two G4 ligand PDPs tethered to the **Ir-1** obtained the final probe **Ir-PDP** (Fig. 1e). The stability of **Ir-PDP** to G4 and the selectivity between G4 and single-stranded oligonucleotides were determined by the G4 melting curve. The phosphorescence lifetime of **Ir-PDP** was significantly increased after being combined with G4. At the same time, the probe's imaging results in cells showed strong and distinct phosphorescent foci in the cytoplasm. In addition, when RNA was degraded, the cytoplasm's phosphorescent foci disappeared. The lifetime distribution map of **Ir-PDP** in the cells can give an overall map of **Ir-PDP** binding events in the cytoplasm. Adding G4 ligand pyridostatin (PDS) to living cells significantly regulated the lifetime in the cytoplasm [10].

Compared to the three Ir(III) complexes (**Ir-1**–**Ir-3**), it was found that, if the electron donor group methyl or the conjugate system was modified on the electron-deficient pyridine group, the phosphorescence emission spectra exhibited bathochromic shifts, whilst phosphorescence intensity weakened (Fig. S1 in Supporting information). These results confirm previous studies [36]. In particular, **Ir-3** had higher absorbance in DMSO solution than **Ir-1** and **Ir-2** at the same concentration at 365 nm, unfortunately, its phosphorescence intensity was the lowest. To ensure that the probe had excellent phosphorescent emission intensity, **Ir-1** was selected as the phosphorescent emitter. The probe **Ir-PDP** was synthesized from **Ir-1** and PDP dehydration to form amide bonds, and purified by HPLC for subsequent experiments (Fig. S2 in Supporting information, and detailed synthesis process and characterization data are listed in the Supporting information). It is worth mentioning that the phosphorescence intensity of **Ir-PDP** is weaker than **Ir-1**, similarly, its maximum emission wavelength is accompanied by a small amount of redshift (Fig. S3 in Supporting information), which presents high requirements for the phosphorescence intensity of iridium(III) complexes before PDP installation.

Furthermore, **Ir-1** and **Ir-PDP** have different phosphorescence properties. At different pH (3.5, 5.0, 6.0, 7.4, 9.0), the phosphorescence intensity of **Ir-1** and **Ir-PDP** vary greatly. The phosphorescence of **Ir-1** disappeared at physiological pH. Nonetheless, it showed relatively high phosphorescence intensity at pH 5.0 (Fig. S4a in Supporting information). **Ir-PDP** showed stronger phosphorescence intensity at physiological pH but weaker phosphorescence intensity at acidic conditions. When the pH was less than 5, the phosphorescence signal of **Ir-PDP** could hardly be detected (Fig. S4b in Supporting information). The opposite phosphores-

cence properties between each other may be related to their terminal groups, which implies the phosphorescence properties of **Ir-PDP** can be expected to respond to the environment of its PDPs.

In different DMSO: Buffer (pH 7.4) ratios, the phosphorescence intensity of **Ir-PDP** kept essentially constant in DMSO and the aqueous phase containing 1% DMSO (Fig. S5a in Supporting information). Additionally, to avoid phosphorescence intensity changes caused by different contents of the Tris-HCl buffer, the phosphorescence intensity changes of **Ir-PDP** not acidified by trifluoroacetic acid were tested in different DMSO: water ratios and similar results were obtained (Fig. S5b in Supporting information).

Given **Ir-PDP** had good phosphorescent emission intensity in an aqueous solution containing 1% DMSO and pH 7.4, we incubated **Ir-PDP** with oligonucleotides formed different secondary structures *in vitro* and found that different nucleic acid secondary structures increased the phosphorescence emission intensity of the probe by about 3∼4 times (Figs. S6a and b in Supporting information), but it was difficult to distinguish them only by the intensity response. Nevertheless, since no phosphorescence change was observed in **Ir-1** in the presence of G4 structure (Fig. S6b), we speculate that the change of phosphorescence intensity of **Ir-PDP** must be caused by the binding of installed G4 ligand PDPs to oligonucleotides.

Given the complex molecular structure of **Ir-PDP**, its ability to stabilize G4 was tested by detecting the melting temperature change of the G4 oligonucleotide sequence [37,38]. First, two DNA G4 and four RNA G4 sequences were annealed in potassium ion and Tris-HCl buffer (10 mmol/L, pH 7.4) solution to form the G4 structure. Then, **Ir-PDP** with 2 equiv. or 4 equiv. oligonucleotide concentration was added. After 1 h of incubation at 20 °C, **Ir-PDP** stabilized the six G4 structures (Fig. S7 in Supporting information). Moreover, increasing the **Ir-PDP** concentration significantly increased the G4 melting temperature (Fig. 2a). To evaluate the stability of **Ir-PDP** to G4 structure, we used the same concentration of PDS, PDP, or **Ir-PDP** combined with folded G4 (c-myc) respectively. After PDS, PDP and **Ir-PDP** were added, similar G4 signals were obtained (Fig. 2b), but **Ir-PDP** made the T_m of G4 more significantly increase (Fig. 2c), so **Ir-PDP** has better stability to G4. It is worth mentioning that by adding the same concentration of PDS in advance to the oligonucleotides folded into the G4 structure, and then adding the same concentration of **Ir-PDP** after they are fully combined, it is found that the G4 structure can be further stabilized (Fig. 2d and Fig. S8 in Supporting information).

Generally, there are two methods to study the interaction between chemical molecules and G4. One is to interact the studied molecules with the folded G4 structure, which is common in the method of studying G4 probes. The other is to anneal the chemical molecules with G4 sequence and K^+ to study the inducing effect of chemical molecules on G4, which is common in some reports of developing new G4 ligands. Since the high-temperature process used during annealing cannot appear in the cell environment, to study the inducing effect of **Ir-PDP** on the G4 sequence, we denatured the G4 sequence at high temperature in advance, and then added it to the prescription we want to study. This protocol is expected to be used to simulate the induction of the probe **Ir-PDP** on the sequence being folded into the G4 structure. Therefore, the folding ability of the G4 sequence induced by **Ir-PDP** was analyzed. First, the G4 sequence was denatured at 95 °C to destroy the secondary structure of oligonucleotides. Then, PDS, **Ir-PDP** + PDS, or potassium ions were added at pH 7.4 (10 mmol/L Tris-HCl buffer). Interestingly, when **Ir-PDP** and PDS existed together, the CD signal generated by G4 folding was higher than when PDS existed alone (Figs. 2e and f). This shows that in a homogeneous environment when there is one PDS and two **Ir-PDPs** near the unfolded G4 sequence, the sequence tends to fold to form a G4 structure. In addition, since **Ir-PDP** has a stronger G4 binding ability than PDS, additional G4 signals are more likely to be provided by **Ir-PDP**.

The excellent ability of **Ir-PDP** to combine G4 provides us with the confidence to develop it into a G4 phosphorescent probe. Firstly, the test of the lifetime of **Ir-PDP** in DMSO and pH 7.4 aqueous solution showed a longer lifetime in the aqueous solution (Fig. 2g). After co-incubation with G4, the lifetime further increased. Using oligonucleotides with different secondary structures showed that, although the single-stranded oligonucleotides increased the lifetime of **Ir-PDP** to a certain extent, the G4 structure could increase the **Ir-PDP** lifetime to more than 200 ns (Fig. 2h and Fig. S9 in Supporting information). Moreover, double-strand and hairpin structures had little effect on the lifetime (Figs. 2g and h). Further, in the system of coexistence of G4 structure and single strand, the probe **Ir-PDP** can selectively bind to G4 and maintain the ability to efficiently increase the T_m of G4 (Fig. S10 in Supporting information). Therefore, considering that **Ir-PDP** can selectively combine G4 structure, and through lifetime imaging instrument, it can distinguish the stronger response of **Ir-PDP** lifetime to G4 [21].

To prove that the additional PDS would not interfere with the phosphorescence lifetime of **Ir-PDP**, the time-resolved phosphorescent decay of **Ir-PDP** was tested with the coexistence of **Ir-PDP** and PDS. It was found that the addition of PDS had no significant effect on the **Ir-PDP** phosphorescence lifetimes (Fig. S11 in Supporting information). Similarly, when K^+, **Ir-PDP** and PDS coexisted, the unfolded G4 sequence was added, and the G4 sequence was folded by the induction of K^+, which produced the obvious CD signal of G4 (Fig. S12 in Supporting information). Then, the phosphorescent emission lifetime of **Ir-PDP** was tested for this hybrid system. And the folded G4 still increased the lifetime of probe **Ir-PDP** by more than 200 ns (Fig. 2i), showing the phosphorescent lifetime signal generated when **Ir-PDP** is combined with G4.

In this case, we hope **Ir-PDP** can be used in intracellular G4 imaging. First, the relative cytotoxicity of different concentrations of **Ir-1** or **Ir-PDP** to MCF-7 cancer cells and MCF-10A normal cells after 24-h incubation was tested. The reduced cytotoxicity could occur because of the steric hindrance of the groups installed on the iridium complex. The MTT protocol showed that the cells still maintained good cell viability when the **Ir-1** or **Ir-PDP** were at 100 μmol/L (Fig. S13 in Supporting information). Then, 20 μmol/L **Ir-PDP** was used to explore its localization in cells. Confocal laser scanning microscopy (CLSM) imaging showed that in both MCF-7 cells and MCF-10A cells, **Ir-PDP** was localized in the cytoplasm relative to the nuclear localization reagent Hoechst 33342 (Figs. 3a and b). Moreover, the probe formed the bright phosphorescent foci in the cytoplasm. Since lysosomes tend to be punctate in the cytoplasm, we then treated cells with **Ir-PDP** and lysosomal fluorescent probe Lyso-Tracker Green (LTG). CLSM imaging showed that LTG and **Ir-PDP** showed insignificant overlap in the cytoplasm of both MCF-7 cells and MCF-10A cells (Figs. 3c and d).

To verify whether the phosphorescence foci were related to nucleic acids in the cytoplasm, we treated fixed MCF-7 cells with DNase I or RNase A. After DNase I treatment, the blue nuclear dye disappeared, but the red phosphorescent foci in the cytoplasm still existed (Fig. 4a), indicating that the phosphorescence foci in the cytoplasm may not be related to the DNA in the cytoplasm. However, when the cells were treated with RNase A, the blue nuclear dye still existed, but the phosphorescence foci in the cytoplasm disappeared (Fig. 4b), and only the weak background in the nucleus could be seen, which is caused by Hoechst 33342 being excited by the laser of the same wavelength with **Ir-PDP**. The largest emission peak of Hoechst 33342 was 461 nm, but there was a weak luminescence signal at 600 nm. Therefore, the luminescence intensity in the cytoplasm is even less than the background of Hoechst 33342 at 600 nm, which supports our argument that the phosphorescence foci in the cytoplasm disappeared. Furthermore, without DNase I and RNase A treatment, the phosphorescence foci formed

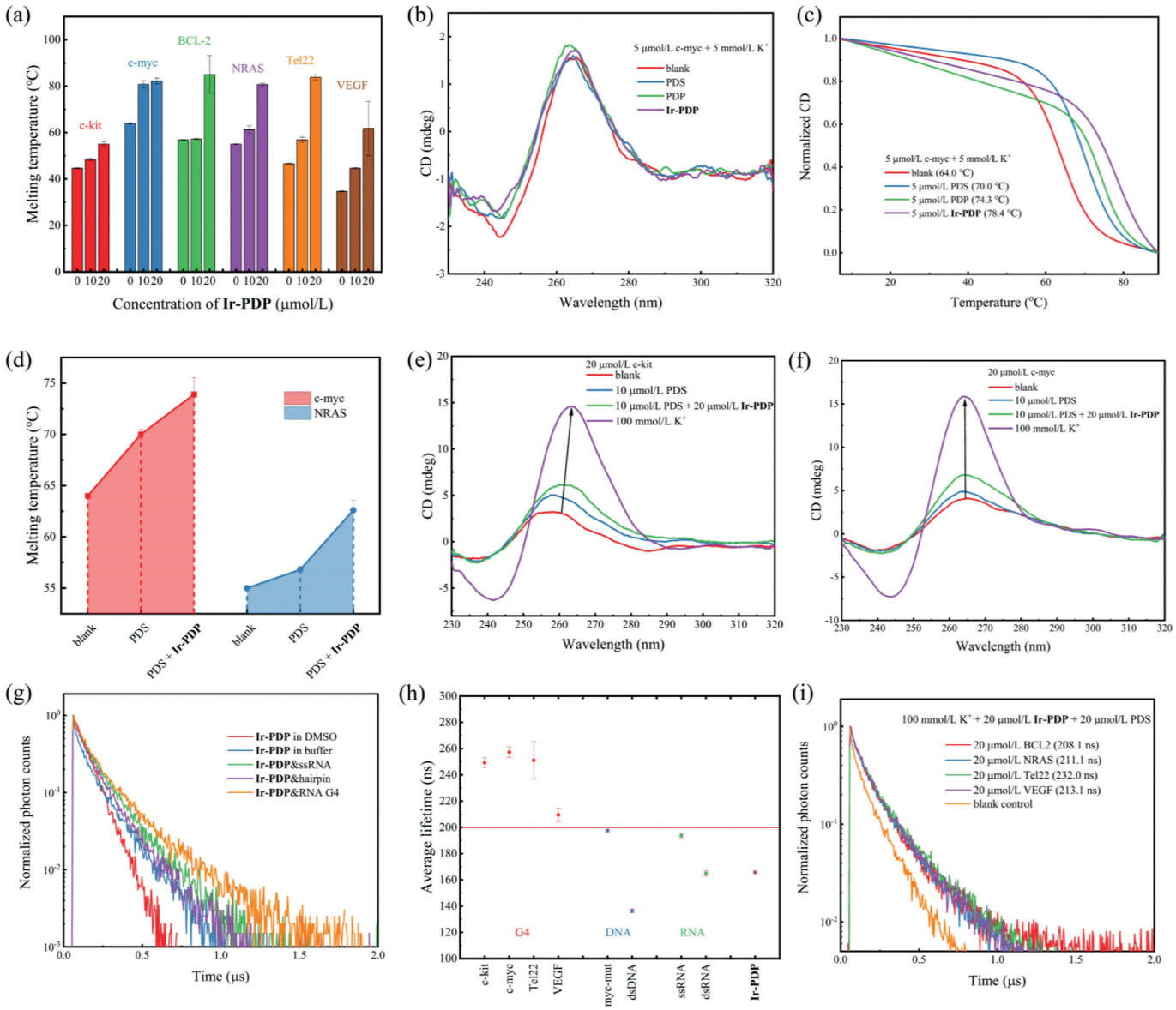

Fig. 2. Interaction between **Ir-PDP** and oligonucleotides *in vitro*. (a) **Ir-PDP** induced a change in the melting temperature of G4, the concentration of the six G4 sequences was 5 μmol/L, and the melting temperature of G4 was tested with the addition of 10 μmol/L or 20 μmol/L **Ir-PDP**. The melting temperature of each G4 is obtained by sigmoid curve + slope fitting, and the error bar is obtained from fitting. (b) CD spectra of 5 μmol/L c-myc in the presence of 5 mmol/L KCl with different ligands. (c) CD melting curves of 5 μmol/L c-myc in the presence of 5 mmol/L KCl with different ligands. (d) T_m of 5 μmol/L c-myc (red) or NRAS (blue) in the presence of 5 mmol/L KCl without ligand and with 5 μmol/L PDS, or 5 μmol/L PDS + 5 μmol/L **Ir-PDP**. (e, f) CD spectra of G4 ligand interacting with G4 sequence. The curve "blank" is that 100 μmol/L of G4 sequence was denatured at 95 °C for 10 min and immediately added to Tris-HCl buffer (pH 7.4) without other components. In addition, PDS (10 μmol/L), PDS + **Ir-PDP** (10 μmol/L + 20 μmol/L) and KCl (100 mmol/L) were added to induce G4 formation. (e): 20 μmol/L c-kit; (f): 20 μmol/L c-myc. (g) Time-resolved phosphorescence decays of **Ir-PDP** in DMSO (10 μmol/L), buffer (10 mmol/L Tris-HCl buffer pH 7.4, 100 mmol/L KCl, 10 μmol/L **Ir-PDP**) or following the subsequent additions of ssRNA (20 μmol/L), hairpin (20 μmol/L) or RNA G4 (Tel22, 20 μmol/L) in above buffer. (h) Lifetime variation of **Ir-PDP** (10 μmol/L) in buffer (pH 7.4, black dots) or in the presence of different G4s (20 μmol/L, pH 7.4, 100 mmol/L KCl), ss/dsDNA (20 μmol/L, pH 7.4, 100 mmol/L KCl) and ss/dsRNA (20 μmol/L, pH 7.4, 100 mmol/L KCl). The error bar comes from the error caused by the exponential fitting. (i) Time-resolved phosphorescence decays of 20 μmol/L **Ir-PDP** in the presence of 100 mmol/L KCl, 20 μmol/L PDS and four different RNA G4s.

in the cytoplasm can completely mask the background generated by Hoechst 33342 at 600 nm (Fig. S14 in Supporting information), and there is a blue signal but no red signal in the nucleus.

Then MCF-7 cells were pretreated with PDS to stabilize the G4 structure in the cells, and next the cells were fixed. After thorough washing, the cells were treated with DNase I or RNase A. Likewise, the phosphorescence foci in the cytoplasm still existed after treatment with DNase I (Fig. 4c), and the phosphorescence foci in the cytoplasm disappeared after RNase A treatment (Fig. 4d). What is more, PDS treatment of cells causes a significant increase in the number of phosphorescence foci compared with the control group without PDS treatment, which indicates that the phosphorescence foci of **Ir-PDP** in the cytoplasm is related to RNA G4. Worth noting that **Ir-PDP** does not have the selectivity of RNA G4 and DNA G4, we suspect that it may be caused by the inability of **Ir-PDP** to contact DNA in the cytoplasm. Therefore, we treated cells with Mito-Tracker Red (MTR) and **Ir-PDP**, as we probably surmised, **Ir-PDP** had inappreciable co-localization with MTR (Fig. S15 in Supporting information).

CLSM imaging confirms that **Ir-PDP** is distributed in living cell cytoplasm and the phosphorescence foci related to RNA G4 is formed. In addition, **Ir-PDP** interaction with G4 significantly im-

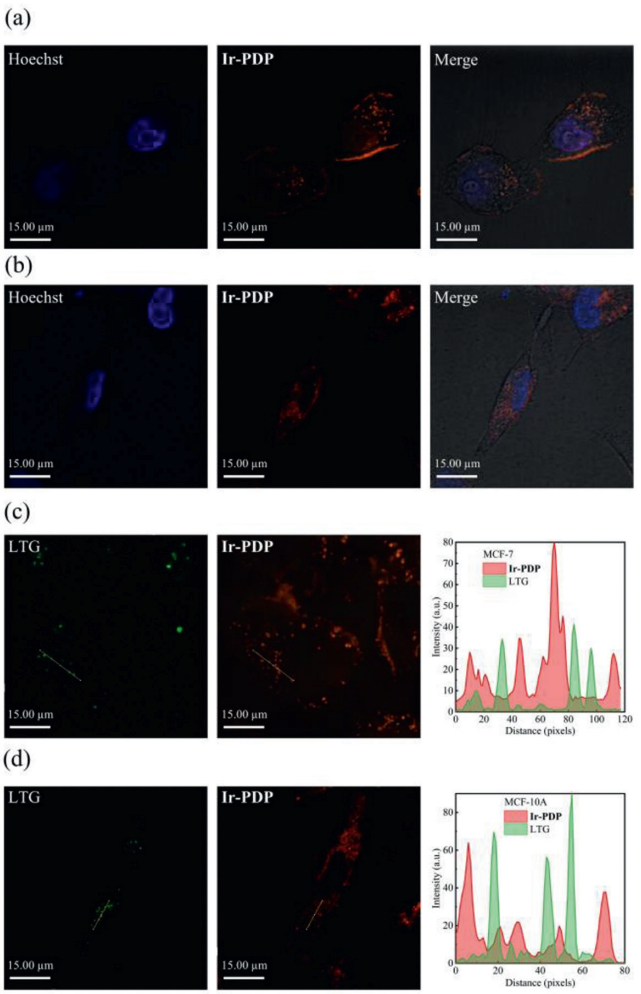

Fig. 3. Confocal laser scanning microscopy imaging of living MCF-7 and MCF-10A cells incubated with **Ir-PDP**. (a, b) Co-localization of **Ir-PDP** (20 μmol/L, 24 h, red) with Hoechst 33342 (10 μg/mL, 20 min, blue) in (a) MCF-7 cells and (b) MCF-10A cells. (c, d) Co-localization of **Ir-PDP** (20 μmol/L, 24 h, red) with LysoTracker Green (50 nmol/L, 20 min, green) in (c) MCF-7 cells and (d) MCF-10A cells. **Ir-PDP**: $\lambda_{ex} = 405$ nm; $\lambda_{em} = 600 \pm 20$ nm. Hoechst 33342: $\lambda_{ex} = 405$ nm; $\lambda_{em} = 447 \pm 20$ nm. LysoTracker Green: $\lambda_{ex} = 488$ nm; $\lambda_{em} = 525 \pm 20$ nm.

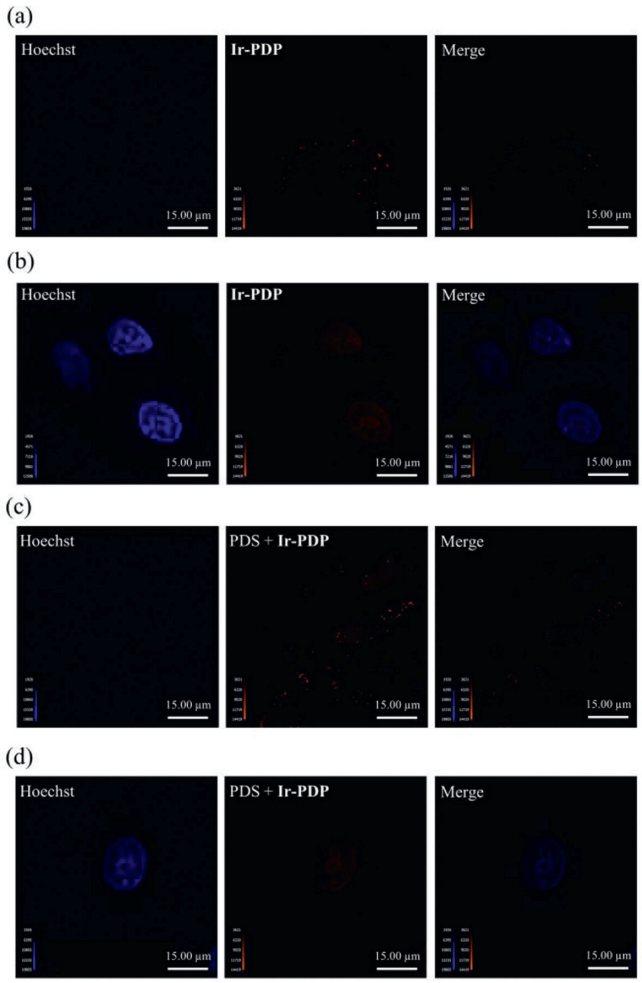

Fig. 4. Confocal laser scanning microscopy imaging of fixed MCF-7 cells. Staining of fixed MCF-7 cells with **Ir-PDP** (20 μmol/L, 12 h, red) and Hoechst 33342 (10 μg/mL, 5 min, blue): (a) pre-treatment with DNase I (100 U/mL, 5 h); (b) pre-treatment with RNase A (1 mg/mL, 5 h); (c) pre-treatment with PDS (10 μmol/L, 12 h) before fixation and then DNase I (100 U/mL, 5 h); (d) pre-treatment with PDS (10 μmol/L, 12 h) before fixation and then RNase A (1 mg/mL, 5 h). **Ir-PDP**: $\lambda_{ex} = 405$ nm; $\lambda_{em} = 600 \pm 20$ nm. Hoechst 33,342: $\lambda_{ex} = 405$ nm; $\lambda_{em} = 447 \pm 20$ nm.

proves its phosphorescence lifetime. We noticed that Zhao and his co-workers established a relationship between the lifetime of an Ir(III) complex and polarity [39]. The greater the polarity, the smaller the phosphorescence lifetime was concluded. However, for **Ir-PDP**, the phosphorescence lifetime in water with high polarity is larger than that in DMSO with low polarity. Therefore, we speculate that the polarity may not be a universal reason for affecting the phosphorescence lifetime. **Ir-PDP** gives much higher affinity with G4 structure through PDP, which promotes the interaction between Ir(III) complex and G4 structure, resulting in the improvement of phosphorescence lifetime. By two-photon excitation at 810 nm, we detected the phosphorescence spectra of **Ir-PDP** (Fig. S16 in Supporting information). Thus, a new sensing pathway about the RNA G4 level in the cytoplasm can be explored by the imaging of two-photon phosphorescence lifetime imaging microscopy (TPPLIM).

First, we treated MCF-7 cells with **Ir-PDP**. Phosphorescence lifetime imaging showed that the phosphorescence lifetime in the cytoplasm was mostly 180~190 ns (Figs. 5a and e), indicating that the binding events between the probe and RNA G4 accounted for only a small part. However, when the cells were treated with **Ir-PDP** and PDS, the phosphorescence lifetime in the cytoplasm increased significantly, more at 220~230 ns (Figs. 5b and f), which revealed that **Ir-PDP** detected the formation of more RNA G4 structures in the cytoplasm. Then, we detected MCF-10A normal cells by the same protocol. The phosphorescence lifetime imaging of MCF-10A cytoplasm showed that the probe lifetime was mainly 220~240 ns (Figs. 5c and g), which indicated that the probe detected more G4 structures. In addition, we also tried to treat cells with **Ir-PDP** and PDS, the phosphorescence lifetime in the cytoplasm was still mainly 220~240 ns (Figs. 5d and h), nevertheless, the lifetime distribution diagram demonstrate that once PDS was added, the phosphorescence lifetime distribution became more concentrated (Figs. 5f and h). In general, the states of G4 sequences in cells can be roughly divided into three categories: the first is unfolded, the second is folded, and the third is combined with other intracellular species. The different states of the RNA G4 sequence will determine that the G4 structure plays different regulatory roles in the cell physiological process. The difference of phosphorescence lifetime imaging between MCF-7 and MCF-10A cells shows that G4 plays different regulatory roles in MCF-7 cancer cells and MCF-10A normal cells. Given the one-day treatment time of **Ir-PDP** in cells, more binding events between **Ir-PDP** and G4 may mean that G4 has more frequent state switching in MCF-10A cells.

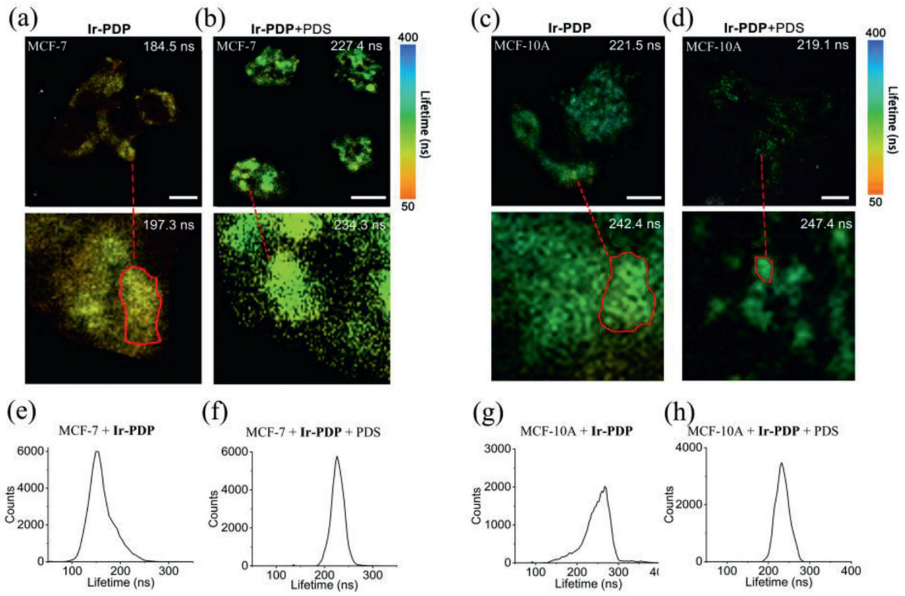

Fig. 5. TPPLIM analysis of lifetime in cancer or normal cells stained with **Ir-PDP**. (a, b) Phosphorescent lifetime imaging in the cytoplasm of MCF-7 cells marked the average lifetime of the analyzed visual field area in the upper right corner of each visual field with (a) **Ir-PDP** (20 μmol/L, 24 h) and (b) PDS (10 μmol/L, 24 h) and **Ir-PDP** (20 μmol/L, 24 h). (c, d) Phosphorescent lifetime imaging in the cytoplasm of MCF-10A cells with (c) **Ir-PDP** (20 μmol/L, 24 h) and (d) PDS (10 μmol/L, 24 h) and **Ir-PDP** (20 μmol/L, 24 h). (e, f) TPPLIM imaging lifetime distribution of living cells: (e) **Ir-PDP** (20 μmol/L, 24 h) in MCF-7cells; (f) PDS (10 μmol/L, 24 h) and **Ir-PDP** (20 μmol/L, 24 h) in MCF-7 cells. (g) **Ir-PDP** (20 μmol/L, 24 h) in MCF-10A cells. (h) PDS (10 μmol/L, 24 h) and **Ir-PDP** (20 μmol/L, 24 h) in MCF-10A cells. **Ir-PDP**: $\lambda_{ex} = 810$ nm (two-photon microscopy); $\lambda_{em} = 600 \pm 20$ nm.

In summary, to provide simple technical support for RNA G4 detection in living cell cytoplasm, we reported a novel G4 phosphorescent probe **Ir-PDP** that emits both in aqueous and organic phases, can stabilize G4 structures, can distinguish different nucleic acid secondary structures through a variation in lifetime, can stay in the cytoplasm of living cells, and can detect the level of RNA G4 in living cell cytoplasm through phosphorescence lifetime imaging. Although G4 in the cytoplasm could not be quantitatively analyzed, compared the phosphorescence lifetime changes of the experimental group treated with PDS and the control group without PDS, we concluded that the G4 structure has a more active state in MCF-10A cells. The sensitive lifetime response of the **Ir-PDP** phosphorescent probe provides new research avenues for the study of G4 structure in the cytoplasm of living cells.

Declaration of competing interest

The authors declare that they have no known competing financial interests or personal relationships that could have appeared to influence the work reported in this paper.

Acknowledgments

This work was supported by the National Natural Science Foundation of China (Nos. 92153303 and 21721005). Thanks to the Wuhan University instrument sharing platform. Thanks to Prof. Shaolong Gong and Prof. Zhen Li of Wuhan University for their FLS9xx spectrometer and Prof. Guangle Niu of Shandong University for their SpectroPro300i spectrameter.

Supplementary materials

Supplementary material associated with this article can be found, in the online version, at doi:10.1016/j.cclet.2022.05.031.

References

[1] D. Sen, W. Gilbert, Nature 334 (1988) 364–366.
[2] G.N. Parkinson, M.P.H. Lee, S. Neidle, Nature 417 (2002) 876–880.
[3] S. Muller, D.A. Sanders, M. Di Antonio, et al., Org. Biomol. Chem. 10 (2012) 6537–6546.
[4] S. Neidle, Nat. Rev. Chem. 1 (2017) 0041.
[5] D. Varshney, J. Spiegel, K. Zyner, D. Tannahill, S. Balasubramanian, Nat. Rev. Mol. Cell Biol. 21 (2020) 459–474.
[6] C. Schaeffer, B. Bardoni, J.L. Mandel, et al., EMBO J. 20 (2001) 4803–4813.
[7] A.L. Wolfe, K. Singh, Y. Zhong, et al., Nature 513 (2014) 65–70.
[8] P. Murat, G. Marsico, B. Herdy, et al., Genome Biol. 19 (2018) 229.
[9] G. Mirihana Arachchilage, A.C. Dassanayake, S. Basu, Chem. Biol. 22 (2015) 262–272.
[10] G. Biffi, M. Di Antonio, D. Tannahill, S. Balasubramanian, Nat. Chem. 6 (2014) 75–80.
[11] S.B. Chen, M.H. Hu, G.C. Liu, et al., J. Am. Chem. Soc. 138 (2016) 10382–10385.
[12] A. Laguerre, K. Hukezalie, P. Winckler, et al., J. Am. Chem. Soc. 137 (2015) 8521–8525.
[13] S. Xu, Q. Li, J. Xiang, et al., Nucleic Acids Res. 43 (2015) 9575–9586.
[14] X. Weng, J. Gong, Y. Chen, et al., Nat. Chem. Biol. 16 (2020) 489–492.
[15] X.C. Chen, S.B. Chen, J. Dai, et al., Angew. Chem. Int. Ed. 57 (2018) 4702–4706.
[16] J. Li, X.C. Yin, B. Li, et al., Anal. Chem. 91 (2019) 5354–5361.
[17] Z. Yu, W. Huang, L. Shi, S. Ke, S. Xu, Chin. Chem. Lett. 33 (2022) 1627–1631.
[18] K.Y. Zhang, Q. Yu, H. Wei, et al., Chem. Rev. 118 (2018) 1770–1839.
[19] M. Di Antonio, A. Ponjavic, A. Radzevicius, et al., Nat. Chem. 12 (2020) 832–837.
[20] A. Shivalingam, M.A. Izquierdo, A.L. Marois, et al., Nat. Commun. 6 (2015) 8178.
[21] P.A. Summers, B.W. Lewis, J. Gonzalez-Garcia, et al., Nat. Commun. 12 (2021) 162.
[22] L.Y. Liu, W. Liu, K.N. Wang, et al., Angew. Chem. Int. Ed. 59 (2020) 9719–9726.
[23] B.C. Zhu, J. He, W. Liu, et al., Angew. Chem. Int. Ed. 60 (2021) 15340–15343.
[24] C.P. Tan, Y.M. Zhong, L.N. Ji, Z.W. Mao, Chem. Sci. 12 (2021) 2357–2367.
[25] L. Hao, Z.W. Li, D.Y. Zhang, et al., Chem. Sci. 10 (2019) 1285–1293.
[26] W.J. Wang, X. Mu, C.P. Tan, et al., J. Am. Chem. Soc. 143 (2021) 11370–11381.
[27] Y.F. Wang, X. Zhang, C.X. Liu, X. Zhou, Acta Chim. Sin. 75 (2017) 692–698.
[28] M. Wang, W. Wang, T.S. Kang, C.H. Leung, D.L. Ma, Anal. Chem. 88 (2016) 981–987.
[29] S. Lin, B. He, C. Yang, et al., Chem. Commun. 51 (2015) 16033–16036.
[30] D. Saadallah, M. Bellakhal, S. Amor, et al., Chem. Eur. J. 23 (2017) 4967–4972.
[31] C. Rajput, R. Rutkaite, L. Swanson, I. Haq, J.A. Thomas, Chem. Eur. J. 12 (2006) 4611–4619.
[32] W.W. Zeng, F. Wu, C.X. Liu, et al., Chem. Commun. 55 (2019) 2269–2272.
[33] H.M. Su, J.L. Xu, Y.Q. Chen, et al., J. Am. Chem. Soc. 143 (2021) 1917–1923.
[34] W. Wang, K.J. Wu, K. Vellaisamy, C.H. Leung, D.L. Ma, Angew. Chem. Int. Ed. 59 (2020) 17897–17902.
[35] K.Y. Zhang, K.K. Lo, Inorg. Chem. 48 (2009) 6011–6025.
[36] A. Tsuboyama, H. Iwawaki, M. Furugori, et al., J. Am. Chem. Soc. 125 (2003) 12971–12979.
[37] S. Paramasivan, I. Rujan, P.H. Bolton, Methods 43 (2007) 324–331.
[38] S. Masiero, R. Trotta, S. Pieraccini, et al., Org. Biomol. Chem. 8 (2010) 2683–2692.
[39] X. Li, X. Tong, Y.H. Yin, et al., Chem. Sci. 8 (2017) 5930–5940.